A Novel Approach To Produce Biologically Relevant Chemical Patterns at the Nanometer Scale: Selective Molecular Assembly Patterning Combined with Colloidal Lithography

Roger Michel,[†] Ilya Reviakine,[†,‡] Duncan Sutherland,[§] Christian Fokas,[‖] Gabor Csucs,[⊥] Gaudenz Danuser,[⊥] Nicholas D. Spencer,[†] and Marcus Textor*,[†]

Laboratory for Surface Science and Technology, Department of Materials, ETH Zurich, Schlieren, Switzerland, Department of Applied Physics, Chalmers University of Technology, Göteborg, Sweden, Laboratory for Organic Chemistry, Department of Chemistry, ETH Zurich, Schlieren, Switzerland, and BioMicroMetricsGroup, Department for Mechanical and Process Engineering, ETH Zurich, Schlieren, Switzerland

A novel patterning technique that combines colloidal patterning with selective adsorption of organic molecules has been used to chemically pattern metal oxide surfaces at length scales down to 50 nm. Lithographic nanofabrication using surface-assembled colloids as etch masks ("colloidal lithography") was used to create nanopillars of TiO_2 (50−90 nm in diameter, ~20 nm in height) on whole oxidized silicon or quartz wafer substrates. These nanopillars were then rendered hydrophobic by the selective self-assembly of an organophosphate, whereas a poly(ethylene glycol)-grafted copolymer was adsorbed onto the surrounding SiO_2 rendering it protein resistant. This resulted in a two-component chemical pattern, displaying contrast with respect to protein adsorption (protein-adhesive pillars on nonadsorbing background). This property allows for efficient translation of the lithographic pattern into a surface protein pattern by two simple dip-and-rinse processes in aqueous solutions. The feasibility of the method and its quality were tested by adsorbing fluorescently labeled streptavidin and biotinylated phospholipid vesicles. The sequential adsorption steps were monitored by fluorescence microscopy, atomic force microscopy, and scanning near-field optical microscopy. These techniques conclusively demonstrated the utility of the described approach for chemical patterning surfaces on the nanometer scale over large areas.

1. Introduction

The biomaterials used today for the fabrication of biomedical devices such as implants are usually not engineered to induce specific biological responses. In particular, the biochemical processes taking place at the interface between the artificial material surface and the bioenvironment are rarely addressed in the surface design. As a consequence, a large variety of proteins and other extracellular matrix components can adsorb to the biomaterial surface in different conformations and orientations. It has been hypothesized that such undefined biofilms are uncommon to nature's biological recognition and immune system, with the effect that the body reacts toward the synthetic material as toward a foreign body.[1] A frequent response of the body to biomaterials is encapsulation and isolation of the implanted device from the blood stream, causing a cascade of reactions that may adversely affect the healing process and the functionality of the device. It is well-known that morphological and topographical features of the biomaterial surface influence the interaction between implant and tissue, most likely through their effect on the proteinacious surface film.[2−6] Improved control over the functional organization of the adsorbed protein layers is therefore one possible approach to improve the ability of the implant to integrate in the host tissue without encapsulation. A key feature of such a strategy would be the elimination or reduction of nonspecific adsorption while at the same time providing chemically and structurally designed interactive sites for the attachment of desirable proteins (such as cell-adhesive proteins) in active conformations. Ultimately, this would imply complete control over the material surface properties on the scale of individual protein molecules.

While a variety of standard techniques is available for engineering of surfaces on the micrometer scale, important advances in nanofabrication technology have only recently opened up new technical solutions to surface engineering on the sub-micrometer scale. Electron-beam lithography, for example, has been successfully used to manufacture nanometer structures with applications ranging from model catalysts[7] to optically active substrates for surface-enhanced Raman spectroscopy (SERS).[8] Such sequential

* To whom correspondence may be addressed at: ETH Zurich, Oberflächentechnik, Wagistrasse 2, CH-8952 Schlieren, Switzerland. E-mail: textor@surface.mat.ethz.ch. Fax: ++41 1 633 10 48.

† Laboratory for Surface Science and Technology, Department of Materials, ETH Zurich.

‡ Current address: Department of Chemical Engineering, University of Houston, Houston, TX.

§ Department of Applied Physics, Chalmers University of Technology.

‖ Laboratory for Organic Chemistry, Department of Chemistry, ETH Zurich.

⊥ BioMicroMetricsGroup, Department for Mechanical and Process Engineering, ETH Zurich.

(1) Ratner, B. D. In *Titanium in Medicine*; Brunette, D., Tengvall, P., Textor, M., Tompson, P., Eds.; Springer: Berlin, 2001, pp 2−12.

(2) Brunette, D. M. In *Surface Characterization of Biomaterials*; Ratner, B. D., Ed.; Elsevier Science Publishers B.V.: Amsterdam, 1988; pp 203−217.

(3) von Recum, A. F.; van Kooten, T. G. *J. Biomater. Sci., Polym. Ed.* **1995**, *7*, 181−198.

(4) Norde, W.; Lyklema, J. *J. Biomater. Sci., Polym. Ed.* **1991**, *2*, 183−202.

(5) Horbett, T. A. In *Proteins At Interfaces*; American Chemical Society: Washington, 1995; Vol. 602, pp 1−23.

(6) Malmsten, M. *J. Colloid Interface Sci.* **1998**, *207*, 186−199.

("writing") techniques, however, suffer from low cost efficiency in the production of large surface areas (>cm^2) with sub-100 nm chemical patterns or structures. Applications of such large-area surfaces include model biomaterial surfaces for protein-surface and cell-surface studies, optimized cell-culture substrates for biotechnology applications in tissue engineering, cell-based sensing assays, functional biochip surfaces for high-sensitivity, high-throughput DNA/RNA and protein detection, and nanoarrays of single molecules for the study of molecular interactions.

Recently, we have developed a novel, simple, and reliable patterning approach, termed selective molecular assembly patterning (SMAP).[9] SMAP is based on the consecutive, selective adsorption from aqueous solutions of dodecyl phosphate to TiO$_2$ and of a polycationic poly-L-lysine-grafted-poly(ethylene glycol) (PLL-*g*-PEG) to SiO$_2$ areas of a prepatterned TiO$_2$/SiO$_2$ substrate. The resulting chemical patterns show a strong contrast with respect to protein adsorption as well as in cell adhesion responses. The hydrophobic DDP/TiO$_2$ areas are interactive and the PLL-*g*-PEG/SiO$_2$ areas are highly resistant to protein adsorption and cell attachment. The power of SMAP arises from exploiting well-established, reliable mass production techniques such as photolithography in order to generate an inorganic oxide prepattern. Subsequently, this pattern is translated into chemical and biological contrast by the application of two simple, gentle, and entirely aqueous-solution-based, hence biocompatible, dip-and-rinse processes. Consequently, SMAP presents a number of advantages over existing patterning technologies such as microcontact printing[10–14] and photodegradation or photoactivation[15] of self-assembled monolayers (SAMs).[9] Since SMAP is based on organic molecule adsorption onto prepatterned surfaces, the lateral resolution should not be limited by the molecular adlayer, as long as the dimensions of the prepattern are larger than the size of the molecules used in the subsequent surface modification steps.

Therefore, the aim of this study is to explore the application of SMAP to dimensions smaller than 100 nm, using colloidal lithography for the inorganic prepatterning step. Colloidal lithography is a recently developed technique that has proved appropriate for the parallel and efficient production of nanometer-sized features on large surface areas.[16–18] It is shown in this paper that the combination of the SMAP technology with colloidal lithography can indeed produce biologically relevant chemical patterns down to 50 nm feature size across large areas.

2. Materials and Methods

2.1. Prepatterning of the Metal Oxide Substrate via Colloidal Lithography. Four-inch silicon ⟨110⟩ (Wafernet GmbH, Germany) and quartz (Schott Guinchard S.A., Yverdon Les Bains, Switzerland) wafers were used as substrates. Both were coated with a 12 nm TiO$_2$ layer using reactive magnetron sputtering of the corresponding metal under controlled oxygen supply (Leybold dc-magnetron Z600 sputtering unit). The coatings were carefully characterized by a number of surface-analytical and optical techniques as described in an earlier paper.[19] The surfaces were rendered positively charged by sequential adsorption of positively and negatively charged polyelectrolyte monolayers using poly(diallyldimethylammonium) chloride (PDDA), molecular weight (MW) 200000–350000 and poly(sodium 4-styrenesulfonate) PSS, MW 70000 (both Sigma-Aldrich, Sweden), adsorbed from 2 wt % solutions for 30 s, rinsed, and dried. A final positively charged outer layer was allowed to form in a 5% aluminum chloride hydroxide solution (Reheis Eire) for 30 s, after which the sample was rinsed and dried. In a subsequent step, negatively charged polystyrene colloidal particles (107 ± 5 nm diameter sulfate-modified latex, Interfacial Dynamics Corporation, USA) were adsorbed to the surface from 0.2 vol % solutions for 60 s, followed by a rinse in high-purity water. The resultant monolayer is well described by the random sequential adsorption (RSA) model,[20] exhibiting a short-range order and a characteristic interparticle spacing. The surfaces were dried carefully under nitrogen flow and annealed on a hotplate for 60 s at a temperature of 116 °C, which is above the glass transition temperature of polystyrene (~106 °C). The samples were then anisotropically etched in an argon ion beam (500 eV ion energy, 0.2 mA/cm^2, 540 s, 10° sample tilt, sample rotation, CAIBE ion beam system, Oxford Ionlab). The layer of immobilized colloidal particles served as a mask during the etching step, protecting locally the TiO$_2$ layer, while the unprotected areas were etched down to the underlying SiO$_2$ layer of the substrate. The particles were subsequently removed by UV/ozone (BHK Inc., California USA) treatment (3 mW/cm^2 at 185 nm) for 60 min. The resulting nanostructured samples of TiO$_2$ pillars on a SiO$_2$ background were stored and cleaned in an oxygen-plasma cleaner (Harrick Scientific Corp., Ossining, NY) for 2 min immediately before use in the SMAP modification steps.

2.2. Selective Molecular Assembly Patterning (SMAP): Conversion of Oxide Material Contrast into Protein-Adhesion Contrast. It has been shown previously that the substrate material contrast (TiO$_2$/SiO$_2$) can be converted into a contrast with respect to protein adsorption by sequentially exposing the samples to aqueous solutions of dodecyl phosphate (DDP) and poly-L-lysine-*g*-poly(ethylene glycol) (PLL-*g*-PEG), thus creating protein-interactive patches on a protein-resistant background.[9]

In particular, the patterned SiO$_2$/TiO$_2$ silicon or quartz wafer substrates were immersed in an aqueous solution of 0.5 mM ammonium dodecyl phosphate (CH$_3$(CH$_2$)$_{11}$PO$_4$(NH$_4$)$_2$),[21] incubated for 24 h, and rinsed with high-purity water, thus producing a well-defined, hydrophobic SAM layer of DDP on the TiO$_2$ patches, while leaving the SiO$_2$ areas entirely uncovered. In a next assembly step, the patterned TiO$_2$/DDP//SiO$_2$ samples were immersed in a 1 mg/mL PLL-*g*-PEG solution in HEPES I buffer (10 mM 4(2-hydroxyethyl)piperazine-1-ethanesulfonic acid, adjusted to pH 7.4 with 6 M NaOH, Fluka) for 15 min,[22] washed with HEPES I buffer and then with water, and either dried in a stream of nitrogen or further modified immediately as described below.

(7) Wong, K.; Johansson, S.; Kasemo, B. *Faraday Discuss.* **1996**, *105*, 237.

(8) Gunnarsson, L.; Bjerneld, E. J.; Xu, H.; Petronis, S.; Kasemo, B.; Kall, M. *Appl. Phys. Lett.* **2001**, *6*, 802–804.

(9) Michel, R.; Lussi, J.; Csucs, G.; Reviakine, I.; Danuser, G.; Hubbell, J. A.; Textor, M.; Spencer, N. D. *Langmuir* **2002**, *16*, 6305–6509.

(10) Bernard, A.; Renault, J. P.; Michel, B.; Bosshard, H. R.; Delamarche, E. *Adv. Mater.* **2000**, *12*, 1067–1070.

(11) Mrksich, M.; Whitesides, G. M. *Trends Biotechnol.* **1995**, *13*, 228–235.

(12) Wilbur, J. L.; Kumar, A.; Kim, E.; Whitesides, G. M. *Adv. Mater.* **1994**, *6*, 600–604.

(13) Bernard, A.; Delamarche, E.; Schmid, H.; Michel, B.; Bosshard, H. R.; Biebuyck, H. *Langmuir* **1998**, *14*, 2225–2229.

(14) Chen, C. S.; Mrksich, M.; Huang, S.; Whitesides, G. M.; Ingber, D. E. *Science* **1997**, *276*, 1425–1428.

(15) Hickman, J. J.; Bhatia, S. K.; Quong, J. N.; Shoen, P.; Stenger, D. A.; Pike, C. J.; Cotman, C. W. *J. Vac. Sci. Technol., A* **1994**, *12*, 607–616.

(16) Sutherland, D. S.; Broberg, M.; Nygren, H.; Kasemo, B. *Macromol. Biosci.* **2001**, *1*, 270–273.

(17) Deckman, H. W.; Dunsmuir, J. H. *Appl. Phys. Lett.* **1982**, *41*, 377–379.

(18) Fischer, U. C.; Zingsheim, H. P. *J. Vac. Sci. Technol.* **1981**, *19*, 881–885.

(19) Kurrat, R.; Textor, M.; Ramsden, J. J.; Boni, P.; Spencer, N. D. *Rev. Sci. Instrum.* **1997**, *68*, 2172–2176.

(20) Adamczyk, Z.; Zembala, M.; Siwek, B.; P., W. *J. Colloid Interface Sci.* **1990**, *140*, 123–137.

(21) Hofer, R.; Textor, M.; Spencer, N. D. *Langmuir* **2001**, *17*, 4014–4020.

(22) Huang, N. P.; Michel, R.; Voros, J.; Textor, M.; Hofer, R.; Rossi, A.; Elbert, D. L.; Hubbell, J. A.; Spencer, N. D. *Langmuir* **2001**, *17*, 489–498.

2.3. Protein Adsorption to the Patterned Substrates. The SMAP-treated samples, prepared as described above, were incubated in 40 μg/mL Oregon Green labeled streptavidin (Molecular Probes, Eugene, OR) in HEPES I solution for 30 min, extensively rinsed with HEPES I buffer, and finally evaluated in buffer using a fluorescence microscope.

2.4. Biotinylated Vesicle Preparation and Adsorption. Solutions of the lipids dioleoyl phosphatidylcholine and dipalmitoyl phosphatidylethanolamine-lc-biotin (Avanti Polar Lipids, Alabaster, AL) in chloroform and chloroform/methanol, respectively, were mixed in a wt/wt ratio of 9:1. The solvent was then evaporated under an argon stream, and the resulting lipidic film was further dried for 30 min in an oven (at room temperature) connected to an oil-free diaphragm-type vacuum pump. The dry film was resuspended in HEPES II buffer (10 mM HEPES, 150 mM NaCl, 2 mM EDTA) at ~60 °C to yield multilamellar vesicles (MLVs). Unilamellar vesicles were prepared by extruding a suspension of MLVs through 200 nm pore diameter filters using a Lipofast extruder (Avestin Inc., Canada). Extrusion was performed at ~60 °C. Vesicle solutions were stored under argon at 4 °C until used. For liposome binding, the samples were first rinsed extensively with HEPES II buffer, then incubated for 30 min with 0.2−0.4 mg/mL solution of unilamellar biotinylated liposomes, rinsed with HEPES II buffer, and observed in wet state (in buffer) under the fluorescence microscope to verify that the streptavidin adsorbed to the DDP-coated TiO$_2$ pillars was not removed upon exposure to the liposome solution. Selected samples were also imaged by atomic force microscopy (AFM) at this stage. After another incubation step using fluorescently labeled streptavidin, which bound to the biotinylated liposomes, the samples were once again observed in buffer solution in the fluorescence microscope and subsequently imaged with the AFM.

2.5. Instrumentation. 2.5.1. Fluorescence Microscopy. Fluorescence microscopy images were acquired with a Zeiss Axioplan2 microscope using a 25× water immersion objective (Plan-Neofluar 25x, 0.8NA). Images were captured with a Kappa DX-3C (Kappa, Gleichen, Germany) cooled CCD camera using a 450−490 band-pass/520 long-pass (Zeiss-09) filter set for Oregon Green. The camera was controlled and the images were analyzed with the AnalySIS program from SIS (Soft Imaging System, Münster, Germany). Images were acquired after each chemical modification step, using the same integration time.

2.5.2. Atomic Force Microscopy. AFM observations were carried out using a Nanoscope IIIa-MultiMode AFM (Digital Instruments, Santa Barbara, CA) equipped with a "J" (120 μm) scanner, in contact mode. The contact-mode fluid cell (Digital Instruments) was washed with sodium dodecyl sulfate and rinsed extensively with ultrapure water before use. The O-ring was not used. Samples were attached to metal disks coated with Teflon adhesive tape ("BYTAC", Norton Performance Plastics Corp., Ohio, USA) using double-sided adhesive tape, following the procedure described in ref 23 and mounted on the AFM scanner. The microscope was allowed to thermally equilibrate for a minimum of 30 min before imaging. The force was maintained at the lowest possible value by continuously adjusting the set point during imaging.[23] Images of bare substrates were recorded either in water or in buffer using oxide-sharpened silicon nitride tips mounted on cantilevers with a nominal force constant of 0.38 or 0.12 N/m. Images of liposomes bound to the nanopatterns were acquired in buffer using softer cantilevers (k = 0.06 N/m) to avoid damage of the soft structures.

2.5.3. X-ray Photoelectron Spectroscopy (XPS). XPS spectra were recorded on a SAGE 100 (SPECS, Berlin, Germany) using nonmonochromatic Mg Kα radiation with a source power of 240 W (12 kV, 20 mA), electron takeoff angle of 90°, and electron-detector pass energies of 50 eV for survey and 14 eV for detailed spectra. In the high-resolution mode, the reference Ag3d$_{5/2}$ photoemission peak has a full width at half-maximum height (fwhm) of 1.0 eV. During analysis, the base pressure remained below 5×10^{-8} mbar. All binding energies were referenced to the C1s contribution (due to adventitious hydrocarbon contamination) at 285.0 eV.

2.5.4. Scanning Near-Field Optical Microscopy (SNOM). The SNOM images were recorded on a modified

(23) Müller, D. J.; Amrein, M.; Engel, A. *J. Struct. Biol.* **1997**, *119*, 172.
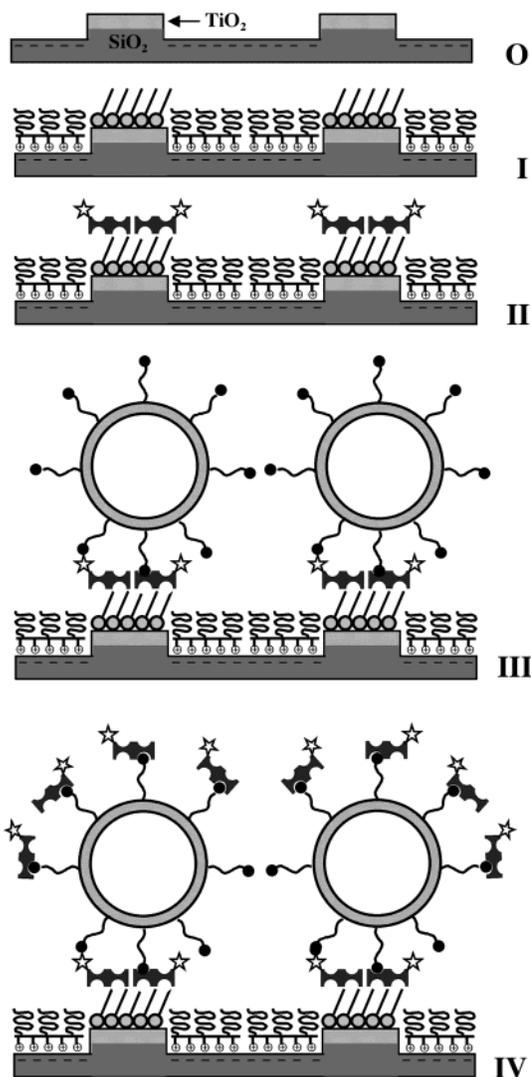

Figure 1. Schematic diagram illustrating the surface architecture and selective molecular assembly pathways applied to surfaces patterned using colloidal lithography: (stage 0) prepatterned substrate generated by colloidal lithography. This results in TiO$_2$ nanopillars on a silicon or quartz substrate; (stage I) same surface after the SMAP treatment (i.e., selective self-assembly of DDP on TiO$_2$ pillars and assembly of PLL-g-PEG on the SiO$_2$ background); (stage II) after adsorption of fluorescently labeled streptavidin adsorbed to the TiO$_2$/DDP nanopillars; (stage III) after immobilization of biotinylated liposomes binding to the streptavidin; (stage IV) after adsorption of fluorescently labeled streptavidin adsorbing onto the biotinylated liposomes.

AURORA (Veeco, Sunnyvale, CA) instrument with a tuning-fork shear-force feedback. In all experiments, the 488 nm line of an argon ion laser with an incident power of 1.5 mW was coupled into the glass fiber tip. The emitted light from the sample was collected by a microscope objective and fed into an avalanche photodiode (Hamamatsu, Shizuoka, Japan). The intense laser line was blocked by a holographic notch filter.

3. Results and Discussion

Surfaces comprised of 20 nm high TiO$_2$ nanopillars on SiO$_2$ background (oxidized silicon or quartz substrate surface, Figure 1, stage 0) were prepared by a combination of colloidal lithography and etching (as described in section 2.1). These TiO$_2$ nanopillars were then modified by self-assembly of the dodecyl phosphate (DDP), while in a second step poly-L-lysine-grafted-poly(ethylene glycol) (PLL-g-PEG) adsorbed onto the SiO$_2$ background (Figure 1, stage
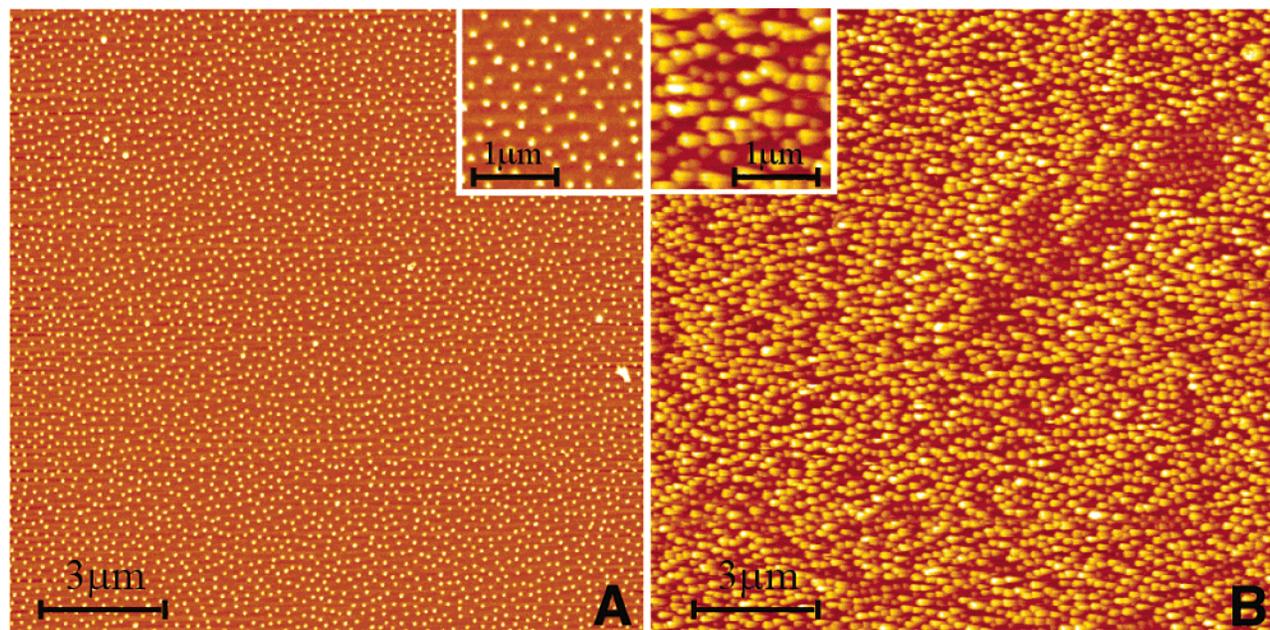
Figure 2. Contact mode AFM images corresponding to steps 0 and IV of the assembly process depicted in Figure 1: (A) bare prepatterned TiO₂/SiO₂ substrate, scan size 15 × 15 μm², Z-scale 75 nm, inset 2.1 × 2.1 μm²; (B) biotinylated liposomes adsorbed to the streptavidin-covered TiO₂/DDP pillars on a SiO₂/PLL-*g*-PEG background. Most of the pillars are covered with the attached liposomes: scan size 15 × 15 μm², Z-scale 200 nm; inset 2.1 × 2.1 μm². It can be seen clearly in the inset that no liposomes are visible between the pillars.

I). Subsequent modification steps included the adsorption of fluorescently labeled streptavidin (Figure 1, stage II), as well as the binding of biotinylated vesicles (Figure 1, stage III). In the latter case a second incubation with fluorescent streptavidin enhanced the fluorescence signal in the vesicle-decorated areas (Figure 1, stage IV). In this study, the biotinylated liposomes were used as markers to decorate the streptavidin that adsorbed to the adhesive TiO₂ nanopillars. This technology can be readily extended to biotinylated vesicles,[24] and thus surface-immobilized vesicles exhibiting widely varying characteristics may be obtained. Special properties of such structures with respect to their ability to incorporate functional transmembrane proteins,[25] encapsulate guest molecules, and form stimuli-responsive structures[26] make surface-immobilized vesicles quite attractive candidates for applications in nanoscale sensing devices, drug delivery systems, etc.

3.1. Characterization of the Prepatterned Substrates. AFM topography images were recorded first to determine the size, height, distribution, and percentage coverage of the TiO₂ pillars on the prepatterned silicon and quartz wafer substrates. A representative AFM image is shown in Figure 2A. The AFM images show 50–90 nm diameter pillars of 20 nm height separated by 200–300 nm. The average TiO₂ pillar diameter was measured with 76 ± 17 nm ($n = 78$ pillars in an area of 2.5 × 2.5 μm², determined via the AFM evaluation software), resulting in a coverage of approximately 5.7%.

Additionally, XPS was used to verify that the prepatterned surfaces indeed exhibit the expected inorganic TiO₂/SiO₂ contrast. Table 1 shows the XPS average atomic concentrations of the elements present in the outermost 5–7 nm for prepatterned, nanostructured silicon and quartz wafer specimens. For both wafer types the patterning was accomplished under identical conditions as

(24) Meier, W. *Langmuir* **2000**, *16*, 1457–1459.
(25) Sauer, M.; Meier, W. *Chem. Commun.* **2001**, 55–56.
(26) Sauer, M.; Streich, D.; Meier, W. *Adv. Mater.* **2001**, *13*, 1649–1651.

Table 1. Surface Composition, As Determined from XPS Measurements, of Unmodified Silicon and Quartz Wafer Substrates Prepared by the Colloidal Lithography Technique (Exhibiting TiO₂ Pillars of 50–90 nm Diameter, 20 nm in Height, Separated by 200–300 nm)[a]

substrate	O (atom %)	Si (atom %)	Ti (atom %)	C (atom %)	% TiO₂ area f_{Ti}
silicon wafer	54.8	43.6[b]	1.6	<1	4.7
quartz wafer	63.7	29.3	1.6	5.4	5.3

[a] Values indicate nominal surface concentration in atom %. The higher silicon and lower oxygen content of the silicon compared to the quartz wafers is due to the fact that the silicon wafer is composed of elemental silicon (Si) as a substrate covered by an approximately 2 nm thick silicon oxide (SiO₂) film, while the quartz wafer has SiO₂ stoichiometry throughout. The fractional area covered by TiO₂ (f_{Ti}) was calculated from the corresponding XPS intensities using standard equations and materials data. [b] Si(2p) peak components indicate 46% Si and 54% SiO₂ of the total peak intensity.

regards the application of the colloidal layer and subsequent etching. Both titanium oxide and silicon oxide were detected at the surfaces of the two wafer types. The higher silicon and lower oxygen content of the silicon compared to the quartz wafer is a direct consequence of their different surface compositions: The silicon wafer is composed of elemental silicon (Si) as a substrate and covered by an approximately 2 nm thick silicon oxide (SiO₂) film. In contrast, the quartz wafer has SiO₂ stoichiometry throughout the substrate. The low hydrocarbon content of both surfaces indicates that the polystyrene particles were indeed removed by the UV/ozone cleaning step following the colloidal patterning process.

The intensities of the Ti(2p) and Si(2p) signals depend, apart from instrumental factors, on the atomic densities of Ti and Si of the substrates used, the ionization cross sections, the mean free path lengths, and the fractional coverage values f_{Ti} and f_{Si} of the two oxides TiO₂ and SiO₂, respectively. With standard equations and material data, f_{Ti} was calculated from the observed XPS intensities to be 0.047 (4.7%) for the prepatterned silicon wafer and 0.053 (5.3%) for the prepatterned quartz wafer (Table 1), in
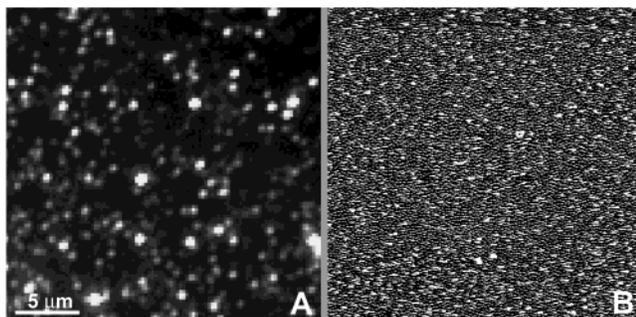
Figure 3. Fluorescence (A) and AFM (B) images of biotinylated liposomes attached to the streptavidin-coated TiO₂ pillars, after incubation with fluorescent streptavidin to label the liposomes. Both images are $25 \times 25 \ \mu m^2$ in size. A distribution of bright spots on a darker background is visible in both images. The spots appear larger in the fluorescence image, due to the significantly lower resolution of this technique (at most 370 nm). They correspond to individual liposomes or clusters thereof, while on the AFM image (B), the bright spots correspond to individual liposomes and the bare pillars are visible in the background. Control experiments, using unlabeled streptavidin, showed no fluorescence above the background value (data not shown).

reasonable agreement with the corresponding mean AFM value (5.7%, see above).

3.2. Chemical Modification: Conversion of Material Contrast into Protein-Adhesion Contrast. The modification of the TiO₂ nanopillars was investigated with two approaches: Since conventional optical microscopy is not capable of resolving <100 nm features, AFM was used to monitor streptavidin and biotinylated vesicle adsorption onto the pillars. Streptavidin was chosen as a model protein due to its chemical and conformational stability as well as for its ability to bind biotinylated species such as biotinylated phospholipid vesicles, which served as markers for the decoration of the streptavidin sites in this study.

3.2.1. Fluorescence Microscopy. In a first set of experiments, fluorescence intensities averaged over an area of $25 \times 25 \ \mu m^2$ were measured on samples at the different, consecutive surface modification stages (Figure 1). Figure 3 shows representative fluorescent microscopy (A) and AFM (B) images, both taken across an area of $25 \times 25 \ \mu m^2$, of a surface at modification stage IV. Due to the limited resolution, fluorescent spots appear larger in the

fluorescent microscopy image in comparison to the size of the vesicles (200 nm diameter). AFM, however, is able to resolve the individual liposomes (bright spots in Figure 3B), demonstrating a rather uniform distribution of the vesicles across the surface. Table 2 shows the average fluorescence intensity values of the surface taken at each of the modification steps I–IV. Unmodified (stage 0) as well as DDP and PLL-*g*-PEG modified (unlabeled) surfaces (stage I) exhibit a background fluorescence signal of 840 ± 20 au. Upon adsorption of fluorescently labeled streptavidin (SA*) onto the hydrophobic, DDP-covered TiO₂ nanopillars (stage II), the signal increases to 1390 ± 190 au. This is a significant, albeit relatively weak signal, as only approximately 5% of the surface area (the TiO₂/DDP/SA* areas) contributes to a fluorescence intensity above background. Upon decoration of the TiO₂/DDP/SA* areas with (unlabeled) vesicles (stage III), the signal intensity is not significantly altered, as expected (1280 ± 210 au). However, upon adsorption of labeled streptavidin SA* to the surface-immobilized biotinylated liposomes (stage IV), the signal intensity once again increases significantly to 3060 ± 400 au. This is expected as each biotinylated vesicle is likely to bind several fluorescent SA* molecules.

3.2.2. Atomic Force Microscopy on the TiO₂ Nanopillars. Atomic force microscopy was used to follow the surface modification steps on individual pillars starting from the unmodified substrates (Figure 2A) to the pillars covered with liposomes (Figure 2B). After the self-assembly of DDP, the pillar height increased from 21.7 ± 0.9 nm to 22.9 ± 1.1 nm (Table 3). This is slightly less than the expected increase of 1.7 nm. (A perfect self-assembled monolayer of a C12-alkane chain with a 30° tilt angle is expected to have a thickness of 1.7 nm[27]). It should, however, be taken into account that electrostatic interactions, changes in surface properties (hydrophobicity), and the degree of perfection of the monolayer will all affect the experimentally observed height difference.

After the adsorption of PLL-*g*-PEG, the height (i.e., the difference between TiO₂ pillar top and surrounding SiO₂ background) is reduced to 21.8 ± 0.7 nm, suggesting that the thickness of the PLL-*g*-PEG layer on SiO₂ is ∼1.1 nm. For comparison, the radius of gyration R_g of the PEG chains, which sets the lower limit on the PLL-*g*-PEG layer thickness, is ∼1.7 nm.[28] One possible explanation for the underestimated layer thickness is the compression of the gel-like PEG layer by the AFM tip.

Table 2. Fluorescence Intensities in Arbitrary Units (a.u.) Taken on the Patterned Surfaces at the Four Different Surface Modification Stages I–IV (According to Figure 1)[a]

	stage I: after DDP and PLL-*g*-PEG adsorption	stage II: plus SA*	stage III: plus biotinyl vesicles	stage IV: plus SA*
fluorescence signal (a.u.)	840	1390	1280	3060
std dev (a.u.)	20	190	210	400

[a] The surface after self-assembly of the dodecyl phosphate (DDP) and poly-L-lysine-grafted-poly(ethylene glycol) (PLL-*g*-PEG) (stage I); after subsequent adsorption of Oregon-Green labeled streptavidin (SA*) (stage II); after the binding of biotinylated vesicles (stage III); and finally again after exposure to SA* to enhance the fluorescence signal in the vesicle-decorated areas (stage IV).

Table 3. Results of the AFM Study on the Development of the Height of TiO₂ Pillars, Taken as the Difference to the Adjacent Silicon Oxide Background, for Samples Treated According to the Series of Surface Modification Steps (See Figure 1)[a]

	stage 0: untreated	stage Ia: after DDP adsorption (to TiO₂)	stage Ib: after PLL-*g*-PEG adsorption (to SiO₂)	stage II: plus streptavidin	stage III: plus vesicles
pillar height (nm)	21.7	22.9	21.8	27.5	61.6
std dev (nm)	0.9	1.1	0.7	0.8	3.5

[a] Molecular assembly of DDP to TiO₂ and PLL-*g*-PEG to SiO₂ (stages Ia and b), streptavidin adsorption to TiO₂/DDP (stage II), and vesicle decoration at TiO₂/SA sites (stage III). Each value was calculated from 10 independent measurements taken randomly across one $2.5 \times 2.5 \ \mu m^2$ AFM image.
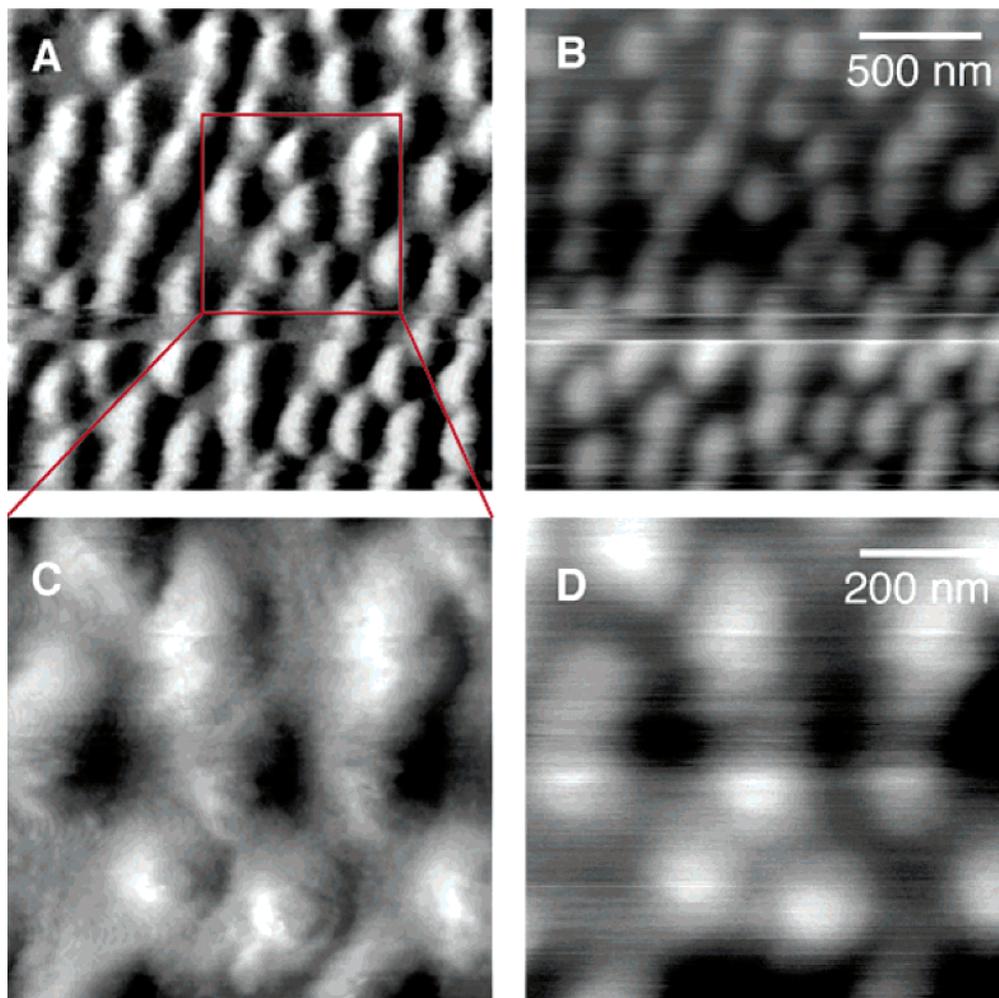
Figure 4. SNOM images of the topography (A) and fluorescence (B) of a SMAP and Oregon-Green labeled streptavidin-treated sample. A magnified scanned region of (C) topography and (D) fluorescence is shown below. The images are displayed without further treatment and show a lateral and chemical contrast of 20−30 nm. The topographical images (A and C, respectively) perfectly coincide with the corresponding fluorescence images (B and D, respectively), indicating that streptavidin has indeed selectively adsorbed onto the ca. 80 nm diameter TiO_2 pillars.

Adsorption of streptavidin and vesicles significantly alters the pillar height to 27.5 ± 0.8 and 61.6 ± 3.5 nm, respectively. These values are qualitatively consistent with the expected increase in pillar height upon adsorption, confirming the selectivity of streptavidin adsorption and liposome binding to the TiO_2 pillars (Figure 2B). The estimate of the thickness of the streptavidin layer (5.7 nm) compares favorably with that previously measured by AFM on lipid monolayers[24] and bilayers[25] and with the dimension of the streptavidin molecule.[26] Vesicle height is underestimated, but the values obtained are consistent with those measured previously in contact mode on mica[29] and on TiO_2.[30] Interestingly, the values measured with tapping mode AFM are larger and reach ∼300 nm for vesicles 200−400 nm in diameter.[31] Therefore, at least one reason for the lower-than-expected values of vesicle height is their deformation by the AFM tip.

3.2.3. Scanning Near-Field Optical Microscopy. For the direct observation of the spatial contrast on the protein level, a state-of-the-art scanning near-field optical microscopy (SNOM) instrument was used to spatially resolve fluorescently labeled streptavidin (SA*) that adsorbed onto the TiO_2 nanopillars.

In Figure 4, a set of SNOM images of the topography and fluorescence intensity are displayed for surfaces after the SMAP-treatment and after the selective adsorption of labeled SA* to the TiO_2/DDP adhesive pillars (stage II). The topographical and optical resolution estimated from Figure 4 lies between 20 and 30 nm. Due to the selectivity of the molecular assembly processes, SA* fluorescence is expected to occur only on the TiO_2 nanopillars and not on the SiO_2 background, as perfectly confirmed by the SNOM data in Figure 4. The topographical image shown in Figure 4A coincides with the fluorescence image in Figure 4B, indicating that SA* has indeed selectively adsorbed onto the TiO_2 pillars.

4. Conclusion

We have developed a simple and versatile sub-100-nm patterning technique that relies on the creation of a coincident oxide material and topographical contrast via colloidal patterning, a lithographic technique suitable for prepatterning whole 4-in. diameter or even larger wafers. The further modification by selective molecular assembly patterning is shown to be appropriate in order to translate

(27) Tamada, K.; Hara, M.; Sasabe, H.; Knoll, W. *Langmuir* **1997**, *13*, 1558−1566.

(28) Kawaguchi, S.; Imai, G.; Suzuki, J.; Miyahara, A.; Kitano, T. *Polymer* **1997**, *38*, 2885−2893.

(29) Reviakine, I.; Brisson, A. *Langmuir* **2000**, *16*, 1806−1815.

(30) Rossetti and Reviakine. Private communications.

(31) Jass, J.; Tjarnhage, T.; Puu, G. *Biophys. J.* **2000**, 79, 3153−3163.

the prepattern into protein-adhesive (TiO$_2$ nanopillars) and protein-resistant (SiO$_2$ background) patterns. These patterns can be decorated with vesicles, which, in turn, can be further functionalized with streptavidin, thus allowing for reactions with any additional biotinylated biomolecules. The simplicity of both the generation as well as the chemical modification of the described structures makes this new methodology a useful supplement to the present nanostructuring toolbox available for biologically motivated research. Using smaller colloids, we intend to produce adhesive areas of less than 10 nm diameter, thus approaching surface architectures suitable for nanoarrays of single macromolecules.

LA0258244